Influence of injection level and wafer resistivity on series resistance of silicon heterojunction solar cells

Léo Basset, Wilfried Favre, Olivier Bonino, Jean-Pierre Vilcot

Topic : 2 - Silicon Materials and Cells
Subtopic : 2.5 - Characterisation & Simulation of Si Cells

Influence of injection level and wafer resistivity on series resistance of silicon heterojunction solar cells

Léo Basset[1], Wilfried Favre[1], Olivier Bonino[1], Jean-Pierre Vilcot[2]
1 : Université Grenoble Alpes, *CEA, LITEN-DTS-LHET*, INES, F-73370, Le Bourget-du-Lac, France
2 : *CNRS – IEMN :* 59650, *Villeneuve d'Ascq, France*
Contact : leo.basset@cea.fr – +334 79 79 27 16

Choice of topic: This work focuses on the modeling and characterization of silicon heterojunction solar cells.

Scientific innovation and relevance: Series resistance (R_S) in SHJ cells is related to various carrier transport mechanisms in both bulk materials and at the interfaces, in combined transverse and lateral directions. We propose to review the influence of wafer dark resistivity on R_S of SHJ cells with the rear emitter configuration and propose a new approach for improved modeling of such devices.

Aim and approach used: Our work aims at improving understanding and modeling of R_S various contributions in SHJ cells with rear emitter configuration. For this purpose, we prepared rear emitter n-type SHJ cells varying the substrate dark resistivity from 0.49 to 14.1 $\Omega.\,\mathrm{cm}$, as well as special samples to allow the measurement of electron contact resistance (ρ_{C,e^-}). We examined variations of effective lifetime, efficiency and series resistance with c-Si dark resistivity.

Results: Efficiency varies only slightly with wafer dark resistivity in our experiment. Injection level is found to be very important to examine performance, both for passivation and series resistance matters. We propose a series resistance model that takes into account the lateral transport in parallel between the c-Si wafer and the ITO layer under varying injection levels.

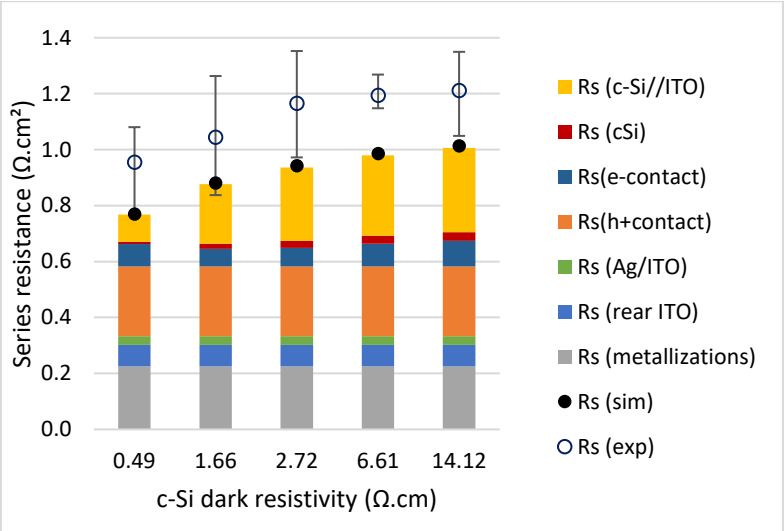

Figure 1 : Measured series resistance of the studied cells as a function of the dark resistivity of the wafer- experimental and simulated results.

Even though a $0.2\Omega.\,cm^2$ gap between our simulation and measured values is observed, our model allows good qualitative agreement with experimental values of R_S, indicating that the experimental variation of R_S for our different batches is explained by an interplay between lateral current and injection level.
More advanced models, as well as variations of other parameters variations with injection level such as electron and hole contact resistivities will be discussed in the final paper.

Summary:

- For high wafer resistivities, a high-injection regime is reached: resistive losses are mitigated by a large c-Si photo-conductivity that allows a large lateral current in the c-Si. But even though very high lifetimes are reached (> 8ms), no increase of V_{OC} or FF are measured.
- For low wafer resistivities, the increased majority carrier density due to high doping allows for better lateral transport in the c-Si, allowing lesser lateral resistive losses, which is reflected as a better fill factor. However, the effective lifetime and injection level at MPP are low, which explains the low V_{OC}'s.

Experiment

A batch of bifacial rear emitter SHJ solar cells were fabricated on CEA SHJ pilot line using n-type Cz wafers of dark resistivity ranging from 0.49 to 14.12$\Omega.cm$. After wafer cleaning and texturing, bi-layers of doped and undoped a-Si:H were deposited by PECVD to form the front surface field (i/n stack) and the rear emitter (i/p stack), followed by ITO deposition on both sides using PVD. Metallization was performed using screen-printing in a 5-busbars design followed by a curing step. A batch of samples (up to PVD step) were cured without metallization for carrier lifetime measurements and TLM samples were produced using screen-printing method for extraction of Ag/ITO contact resistance and electron contact resistance. I-V parameters and pFF were extracted from the finished cells using Chroma solar simulator and SunsVoc tools respectively.

Cells main parameters are presented in Figure 2. We find almost constant efficiency with varying c-Si resistivity: cells made using wafers with low dark resistivity suffer from Voc and Isc drop compensated by higher FF while the cells with high dark resistivity wafers show better Voc and Isc but reduced FF.

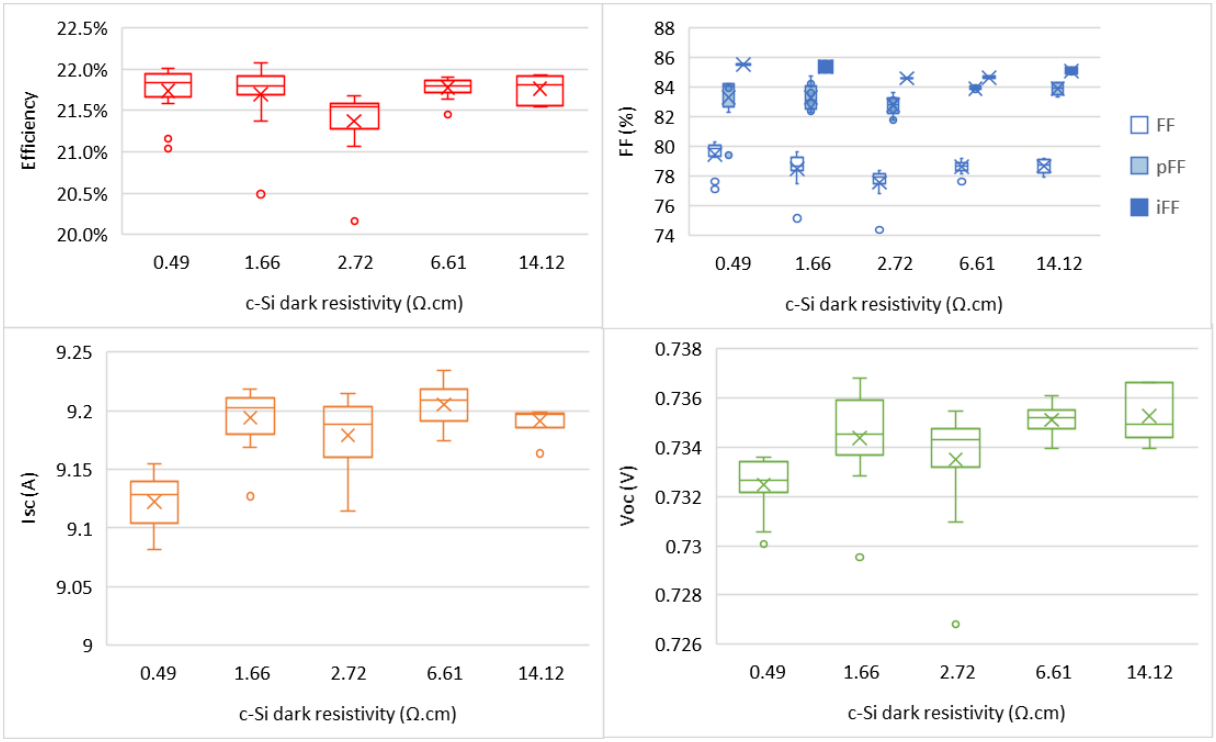

Figure 2 : Cell parameters for the different resistivity classes - iFF values are for post curing samples

Considerations on injection level

Minority carriers effective lifetimes vs injection level obtained from QSSPC technique are presented on Figure 3, for the different dark resistivity samples after curing step. We find that the samples with the lowest dark resistivity suffer from reduced lifetime values over the full injection range, in phase with the lower V_{OC} results at cell level. We also clearly observe a large change of behavior at low injection levels when modifying the wafer dark resistivity.

In Figure 3, we also depicted the minority carrier density at maximum power point (MPP) and open-circuit voltage (OC) for the different cells, calculated from their doping and voltages V_{mpp} and V_{OC}

$$\Delta p_{MPP,OC} \cong \frac{-N_D \pm \sqrt{N_D^2 + 4n_i^2 \exp\left(\frac{q}{nkT} * V_{mpp,OC}\right)}}{2} \qquad eq.(1)$$

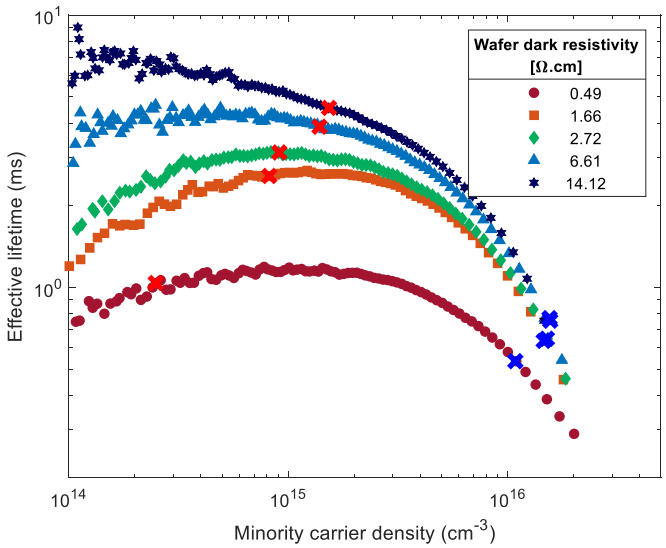

Figure 3 : Lifetime as a function of minority carrier density for the different resistivity classes of post-curing cell precursors. Also plotted are lifetimes at minority carrier densities at MPP (red) and Voc (blue) functioning points

From eq. (1), we can estimate the resistivity of the wafers under working conditions (1Sun MPP, 25°C) using:

$$\frac{1}{\rho_{1Sun,MPP}} = q\left((N_D + \Delta p) * \mu_n + \Delta p * \mu_p\right) \quad eq.(2)$$

In Figure 4 (a), we can see that devices made using low resistivity wafers stay in the low-injection regime ($N_D >> \Delta p$), their resistivity at MPP being close to their dark resistivity (close to 1:1 curve in Figure 4 (b)). In the contrary, devices with lowly doped wafers reach high injection regime at MPP, their resistivity being largely reduced compared to dark conditions.

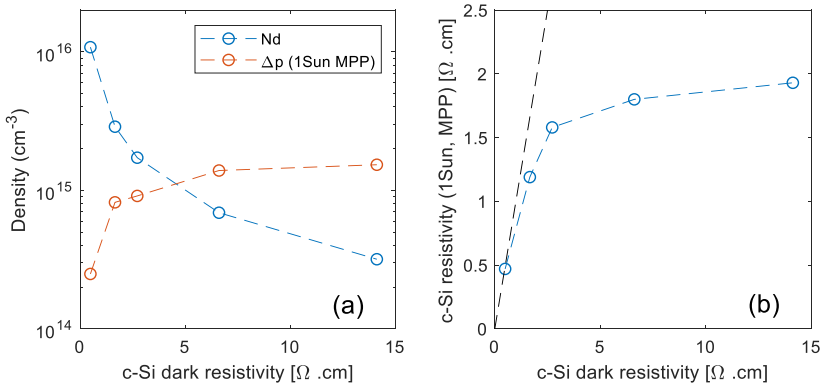

Figure 4 : (b) Doping and minority carrier density at MPP as of function of wafer dark resistivity; (c) resistivity in working conditions as a function of c-Si dark resistivity (blue), black dotted line represents a slope of 1.

Series resistance

We determined the R_S from the median values of IV cells parameters of each split such as :

$$R_S = (pFF - FF) * \frac{V_{OC}J_{SC}}{J_{mp}^2} \quad eq.(3)$$

Figure 5 shows that Rs increases with wafer resistivity from 0.96 to 1.16 $\Omega.cm^2$, and stabilizes after the 2.72 $\Omega.cm$ class reaching 1.21 $\Omega.cm^2$ for the 14.12$\Omega.cm$ class.

We saw that due to high injection, the c-Si resistivity under 1Sun MPP conditions stays quite low even with high wafer dark c-Si resistivities. Bivour et al. [1] showed that the front effective sheet resistance in rear emitter devices can be expressed as

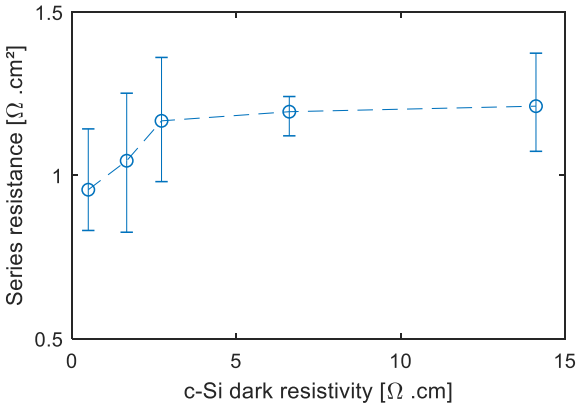

Figure 5 : Evolution of series resistance for solar cells from batches of different wafer resistivity

$\left(\frac{1}{R_{Sh,ITO}}+\frac{1}{R_{Sh,c-Si}}\right)^{-1}$, c-Si playing a part in lateral conduction. Using 4PP technique, we find $R_{Sh,ITO} = 255 \pm 8\ \Omega/sq$ on ITO deposited on glass and submitted to curing, after correction by the 1.4 thickness ratio between textured and polished surface. For silicon, we calculate:

$$R_{Sh,c-Si} = \frac{\rho_{1Sun,MPP}}{t} \rightarrow \begin{cases} R_{Sh_{0.49\Omega.cm}} = 30\ \Omega/sq \\ R_{Sh_{14.1\Omega.cm}} = 120\ \Omega/sq \end{cases} \qquad eq.(4)$$

The sheet resistance of the c-Si under working conditions is much lower than that of the ITO, even for high dark resistivity samples. Therefore, there is a large lateral current in the c-Si base whatever its dark resistivity.

Following a classical approach [2], front lateral carrier transport can be modelled considering the effective sheet resistance under 1Sun MPP [3]:

$$R_S(front\ lateral) = \frac{1}{12} * p^2 * \left(\frac{1}{R_{Sh,ITO}} + \frac{1}{R_{Sh,c-Si}(\Delta p)}\right)^{-1} \qquad eq.(5)$$

To allow full Rs modeling, we characterized the electron contact resistivity (ρ_{C,e^-}) under dark conditions for these samples and found a value below $100\ m\Omega.cm^2$ for all samples, with limited variation with c-Si doping (see Figure 5). The hole contact resistivity (ρ_{C,h^+}) was measured on samples with p-type substrates following the method described in [4], and a value of $250 \pm 50\ m\Omega.\mathrm{cm}^2$ under dark conditions was found.

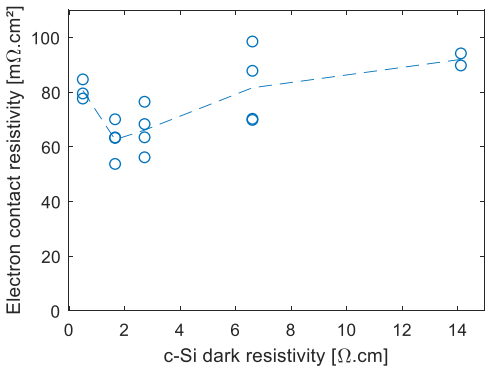

Figure 5 : Electron contact resistivity as a function of c-Si wafer resistivity

As suggested in [4], the series resistance stemming from the contact resistances at the electron and hole contacts can be evaluated with equations (6) & (7).

$$R_S(\text{electron contact}) = \rho_{C,e^-} \qquad eq.(6)$$

$$R_S(\text{hole contact}) = \rho_{C,h^+} \qquad eq.(7)$$

Equation (5) is used to measure the impact of lateral transport, taking into account variations of the ρ_{cSi} with doping and injection level. Finally the contributions from the grid, rear ITO, vertical c-Si transport and Ag/ITO contact resistance is considered, using common R_S power loss analysis [2]. Results are shown in Figure 1.

This model allows good qualitative agreement with measured Rs. Additional features of the SHJ cell transport may help to reach a quantitative agreement e.g. it was reported that hole & electron contact resistivities depend on the injection level [5], [6]. The $0.2\Omega.cm^2$ gap between our simulation and measured Rs may be explained by the increase of ρ_{C,e^-} with increasing injection level. Alternative models and the effect of illumination on R_S and ρ_{C,e^-}will be discussed in the full paper.

[1] M. Bivour, S. Schröer, M. Hermle, and S. W. Glunz, "Silicon heterojunction rear emitter solar cells: Less restrictions on the optoelectrical properties of front side TCOs," *Sol. Energy Mater. Sol. Cells*, vol. 122, pp. 120–129, Mar. 2014.

[2] A. Mette, "New Concepts for Front Side Metallization of Industrial Silicon Solar Cells." 2007.

[3] L. Basset, W. Favre, D. Muñoz, and J.-P. Vilcot, "Series Resistance Breakdown of Silicon Heterojunction Solar Cells Produced on CEA-INES Pilot Line," *35th Eur. Photovolt. Sol. Energy Conf. Exhib. 721-724*, 2018.

[4] D. Lachenal *et al.*, "Heterojunction and Passivated Contacts: A Simple Method to Extract Both n/tco and p/tco Contacts Resistivity," *Energy Procedia*, vol. 92, pp. 932–938, Aug. 2016.

[5] D. Lachenal *et al.*, "Optimization of tunnel-junction IBC solar cells based on a series resistance model," *Sol. Energy Mater. Sol. Cells*, vol. 200, p. 110036, Sep. 2019.

[6] L. Basset, "The Role of Illumination and Temperature on the Electronic Properties at the Front Surface Field Interface of Silicon Heterojunction Solar Cells," ICANS 2019, 2019.